Loss of memory in $H + CH_4 \rightarrow H_2 + CH_3$ state-to-state reactive scattering

Supporting information

Ralph Welsch[1,*] and Uwe Manthe[1,†]

[1] *Theoretische Chemie, Fakultät für Chemie, Universität Bielefeld, Universitätsstr. 25, D-33615 Bielefeld, Germany*

(Dated: December 17, 2014)

Numerical details and convergence test

The present calculations of the state-to-state reaction probabilities employed wavefunction data from previous calculations of thermal rate constants and initial state-selected reaction probabilities[1–3]. Thus, here only the propagation of the thermal flux eigenstates in the product channel has to be discussed.

The curvilinear coordinate system and the kinetic energy operator used for this purpose are taken from Ref. 4. The definition of the coordinate system employs the Jacobi vector $\mathbf{R}'$ pointing from the center of mass of methyl to the center of mass of the H_2, the distance vector of H_2, $\mathbf{r}'$, and a 3+1 Radau construction to describe the methyl fragment. The coordinates used to describe the methyl fragment are identical to the ones used in the description of the reactant channel. They have been introduced and discussed in detail in Ref. 5. The umbrella motion and the *e*-symmetric bends of the methyl are described by the three coordinates θ, χ and ϕ. The symmetric and asymmetric stretching coordinates of the methyl, ρ, ϑ_ρ, and φ_ρ, respectively, are obtained from a spherical parameterization of the norms of the three Radau vectors. The body fixed coordinate system is tied to the methyl fragment. The trisector of the three Radau vectors defines the z-axis and one of the Radau vectors is fixed in the x-z-plane. The Jacobi vectors $\mathbf{r}'$ and $\mathbf{R}'$ are parameterized using stereographic coordinates. The resulting coordinates are denoted r', s', t' and R', S', T'.

The wavefunction representation used in the multi-layer MCTDH calculations is specified in Tabs. I and II and in Fig. 1. Tab. I describes the time-independent basis sets used in the representation of the single-particle functions (SPFs). The design of the multi-layer MCTDH wavefunction representation is depicted diagrammatically in Fig. 1 (see Ref. 6 for a detailed explanation of the diagrammatic notation). The number of SPFs used in the different MCTDH calculations discussed below are specified in Tab. II. The final results presented in the article employ basis 'B'.

The final vibrational state analysis is performed at R'=600 a.u.. Two quartic absorbing potentials are used in the calculation. The absorbing potential decoupling the reactant channel is placed at r'=80 a.u. with a length of 42 a.u. and a maximum strength of $-i\cdot$ 10.368 eV. A second one is placed in the product asymptotic area at R'=1940 a.u. with a length of 60 a.u. and a maximum strength of $-i\cdot$ 10.368 eV. Tests showed that both absorbing potentials do not influence the results. For the projection onto the vibrational

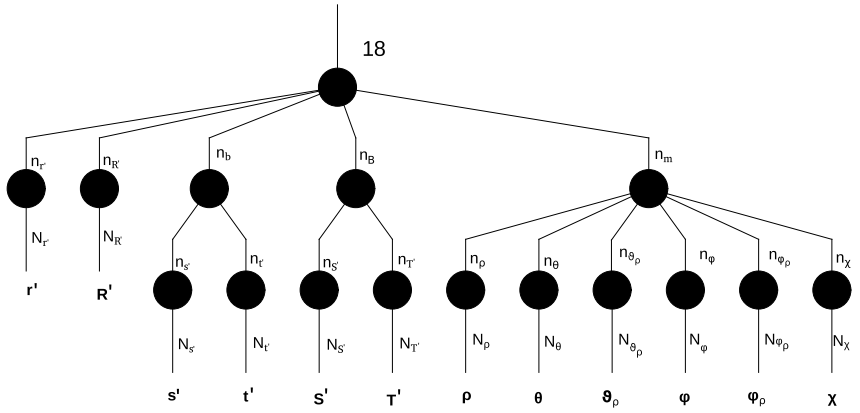

FIG. 1: Diagrams specifying the ML-MCTDH wave function representations employed in the real time propagation.

coordinate	type	size	range
r'	FFT	28	5 - 120
R'	FFT	464	10 - 2000
s', t'	FFT	128	-5.0 - 5.0
S', T'	FFT	208	-5.0 - 5.0
ρ	Hermite-DVR	8	
θ	Hermite-DVR	48	
ϑ_ρ, φ_ρ	Hermite-DVR	8	
φ, χ	Hermite-DVR	8	

TABLE I: Time-independent discrete variable representation (DVR) or fast Fourier transform (FFT) basis sets used to represent the SPF. Coordinate ranges are given in dimensionless units for s', t', S', T' and in atomic units for the mass-weighted distance coordinates r' and R'.

product states, 36 vibrational eigenstates of methyl and 3 vibrational eigenstates of H_2 are calculated for J=0 using the high level ab initio PESs of Refs. 7 and 8, respectively.

To establish the convergence of the SPF basis employed in the MCTDH calculations, different SPF basis sets have been designed (see Tab. II). The smallest basis set is denoted **s**. The basis sets **A**, **B**, **C**, **D**, and **E** increase the number of SPFs employed in the sets of coordinates (r',R',θ), (s',t',S',T'), (ϕ,χ), (ρ), and (ϑ_ρ,φ_ρ), respectively. The number of SPFs employed in the logical coordinates at the upper layers of the "representation tree"

	s	**A**	**B**	**C**	**D**	**E**
$n_{r'}$	6	7	6	6	6	6
$n_{R'}$	13	15	13	13	13	13
n_m	10	12	10	12	11	12
n_ρ	1	1	1	1	2	1
n_θ	8	10	8	8	8	8
n_{ϑ_ρ}, n_{φ_ρ}	1	1	1	1	1	2
n_φ, n_χ	2	2	2	3	2	2
n_b	15	15	21	15	15	15
$n_{s'}$, $n_{t'}$	8	8	10	8	8	8
n_B	15	15	21	15	15	15
$n_{S'}$, $n_{T'}$	8	8	10	8	8	8

TABLE II: The number of SPFs used in the real time propagation with different basis sets. The corresponding multi-layer wavefunction representation is diagrammatically depicted in Fig. 1.

(see Fig. 1) is simultaneously increased to match the change in the bottom layer SPF basis. Comparing the results computed using the basis sets **A** to **E** with results obtained with basis **s**, the convergence can be systematically studied.

State-to-state reaction probabilities calculated employing the different basis sets are displayed in Figs. 2-11. In these figures, results computed with the basis sets **A** to **E** (solid lines) are compared to results obtained with the smaller basis **s** (dashed lines). Figs. 2-6 and 7-11 show results for methane in the initial rotational states j=0 and j=5, respectively, and can be compared to Figs. 1 and 2 of the main article. While Figs. 1 and 2 of the main article display many different reaction probabilities, only non-vanishing state-to-state reaction probabilities are shown in Figs. 2-11. The figures demonstrate the good agreement between the results computed with the different basis sets. Convergence errors not exceeding 10 % are found.

FIG. 2: State-to-state reaction probabilities $p_{\nu_{CH_3},\nu_{H_2}\leftarrow\nu_{CH_4},j=0}(E)$ and initial state-selected reaction probabilities $p_{\nu_{CH_4},j=0}(E)$ computed employing the SPF bases **A** (solid lines) and **s** (dashed lines)

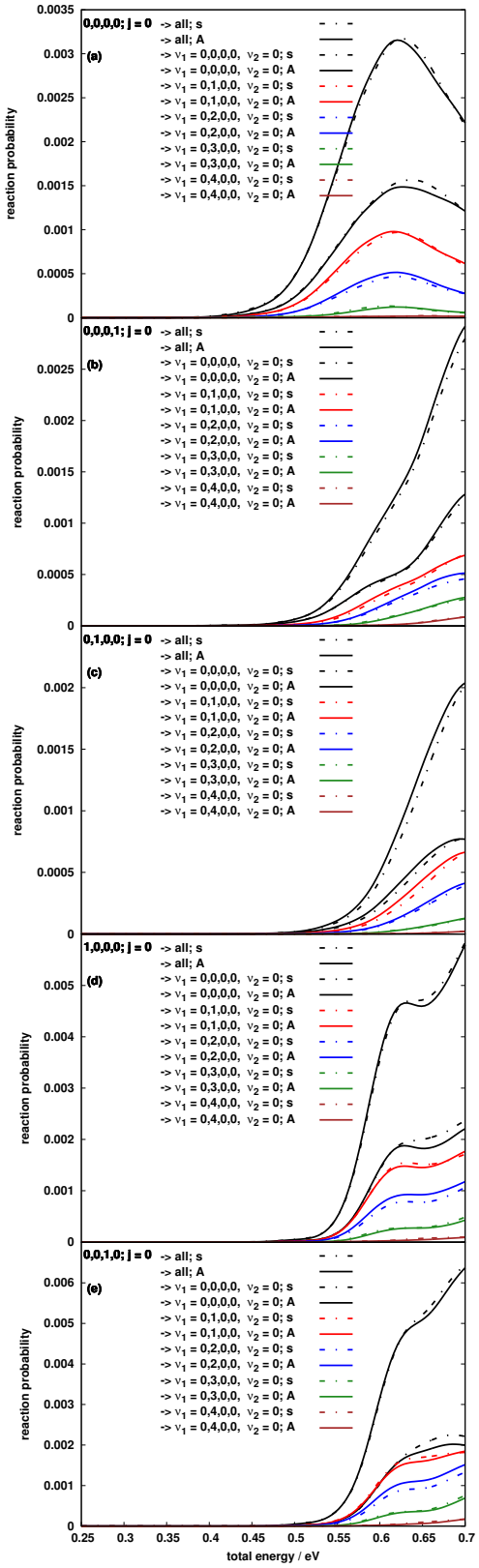

FIG. 3: State-to-state reaction probabilities $p_{\nu_{CH_3},\nu_{H_2}\leftarrow\nu_{CH_4},j=0}(E)$ and initial state-selected reaction probabilities $p_{\nu_{CH_4},j=0}(E)$ computed employing the SPF basis **B** (solid lines) and **s** (dashed lines)

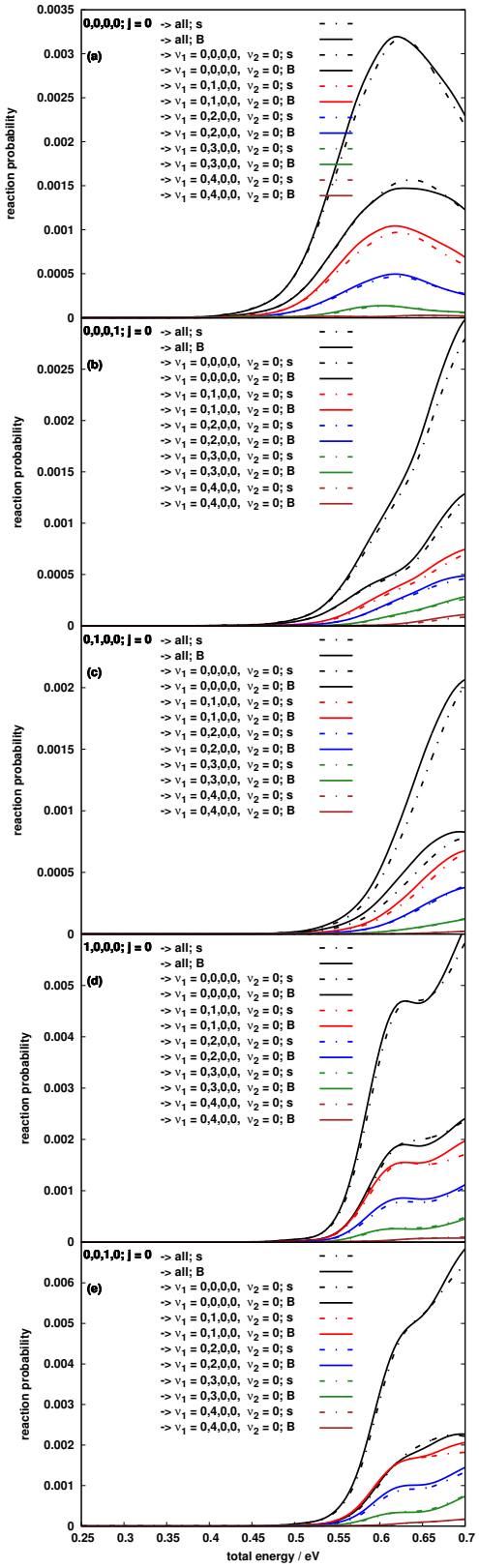

FIG. 4: State-to-state reaction probabilities $p_{\nu_{CH_3},\nu_{H_2}\leftarrow\nu_{CH_4},j=0}(E)$ and initial state-selected reaction probabilities $p_{\nu_{CH_4},j=0}(E)$ computed employing the SPF basis **C** (solid lines) and **s** (dashed lines)

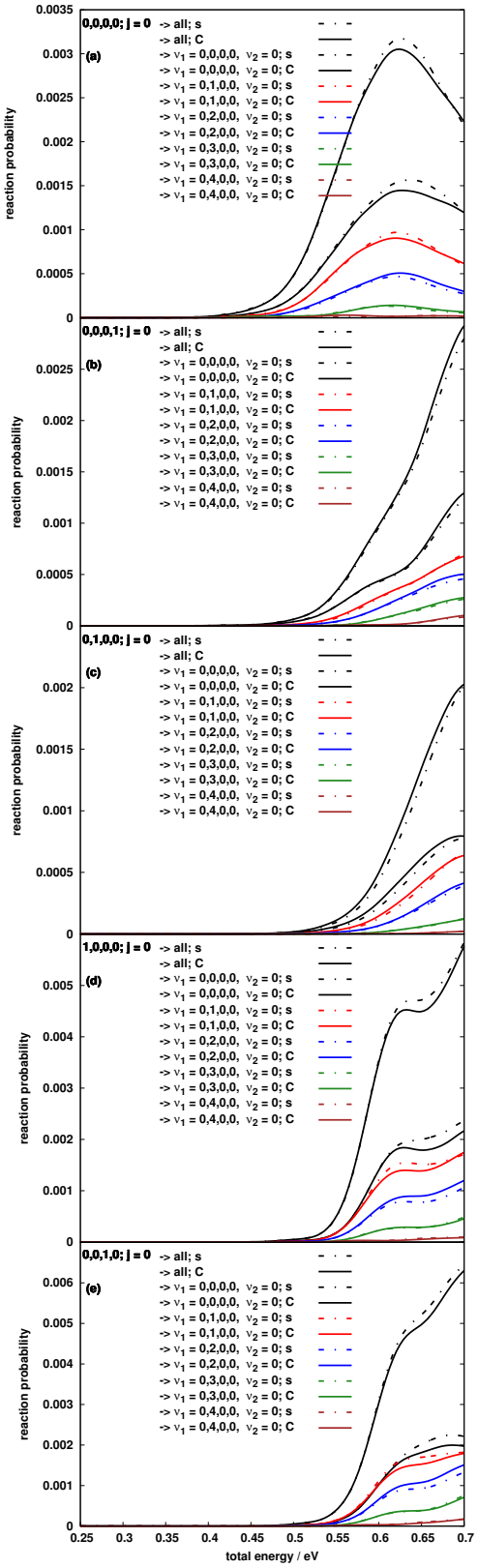

FIG. 5: State-to-state reaction probabilities $p_{\nu_{CH_3},\nu_{H_2}\leftarrow\nu_{CH_4},j=0}(E)$ and initial state-selected reaction probabilities $p_{\nu_{CH_4},j=0}(E)$ computed employing the SPF basis **D** (solid lines) and **s** (dashed lines)

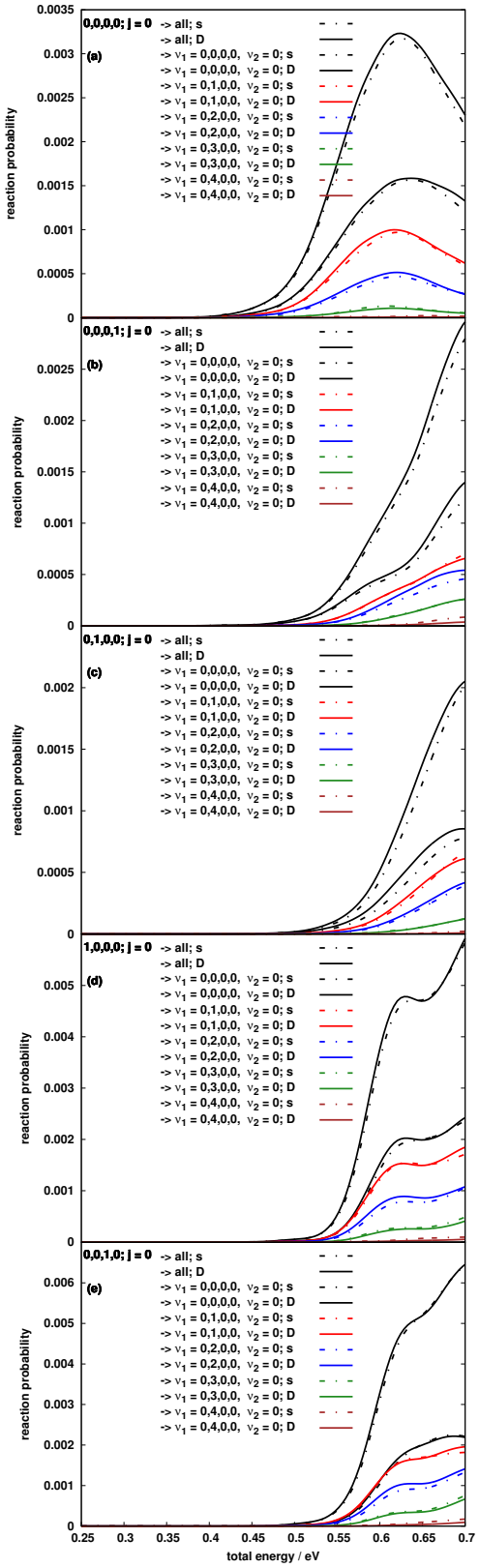

FIG. 6: State-to-state reaction probabilities $p_{\nu_{CH_3},\nu_{H_2}\leftarrow\nu_{CH_4},j=0}(E)$ and initial state-selected reaction probabilities $p_{\nu_{CH_4},j=0}(E)$ computed employing the SPF basis **E** (solid lines) and **s** (dashed lines)

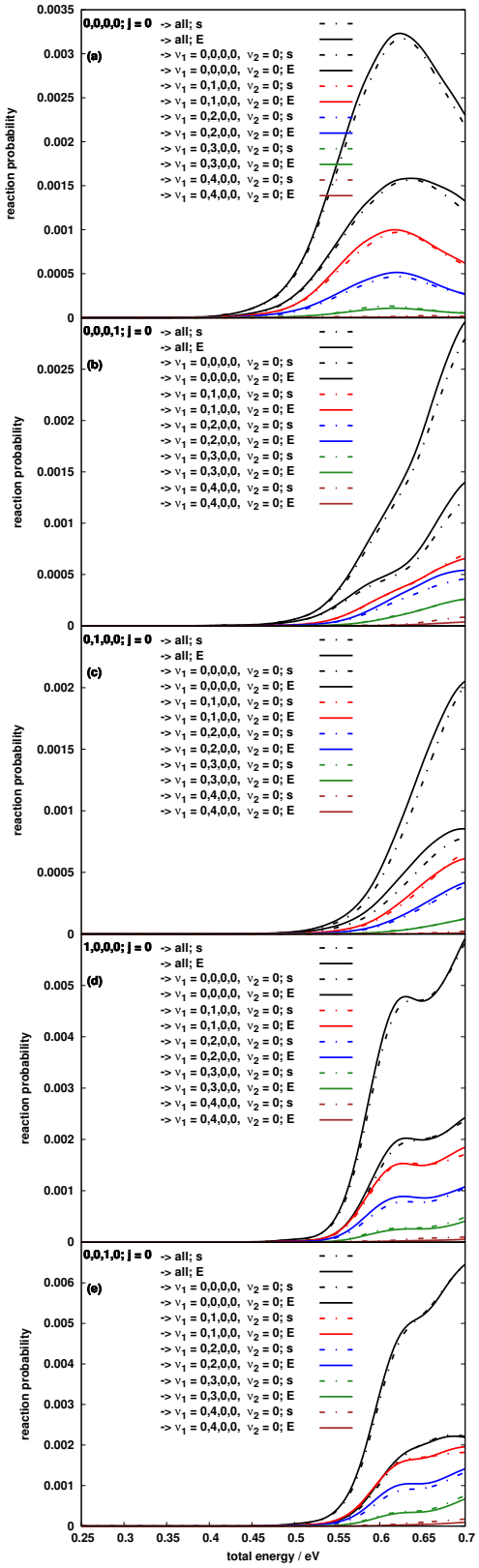

FIG. 7: State-to-state reaction probabilities $p_{\nu_{CH_3},\nu_{H_2}\leftarrow\nu_{CH_4},j=5}(E)$ and initial state-selected reaction probabilities $p_{\nu_{CH_4},j=5}(E)$ computed employing the SPF bases **A** (solid lines) and **s** (dashed lines)

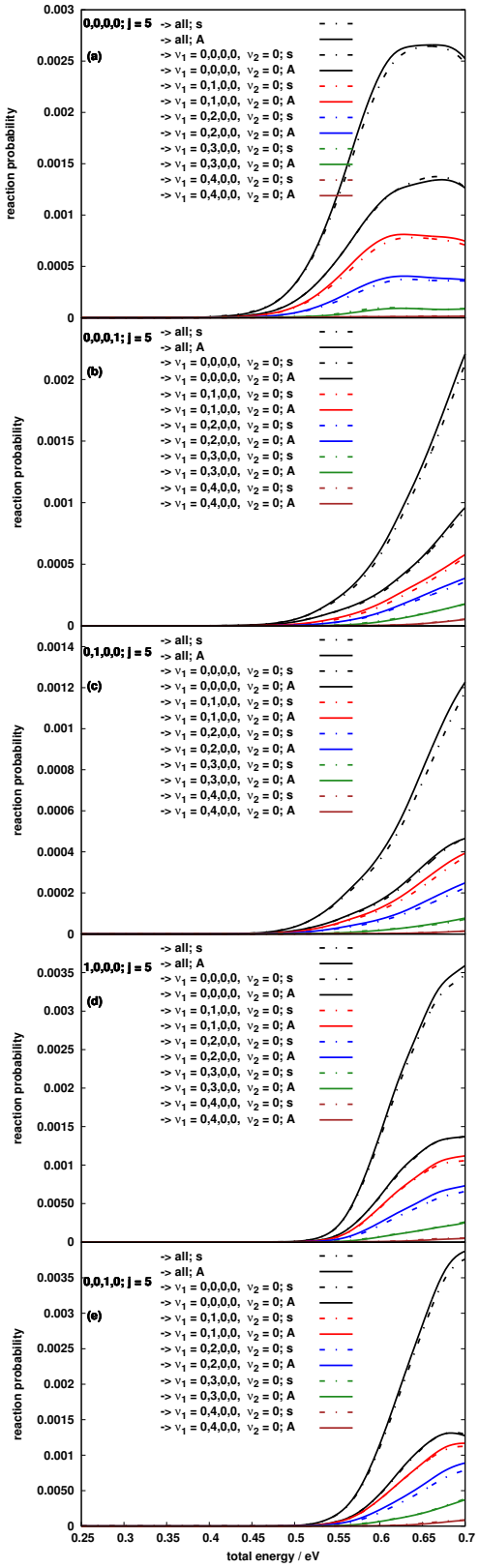

FIG. 8: State-to-state reaction probabilities $p_{\nu_{CH_3},\nu_{H_2}\leftarrow\nu_{CH_4},j=5}(E)$ and initial state-selected reaction probabilities $p_{\nu_{CH_4},j=5}(E)$ computed employing the SPF basis **B** (solid lines) and **s** (dashed lines)

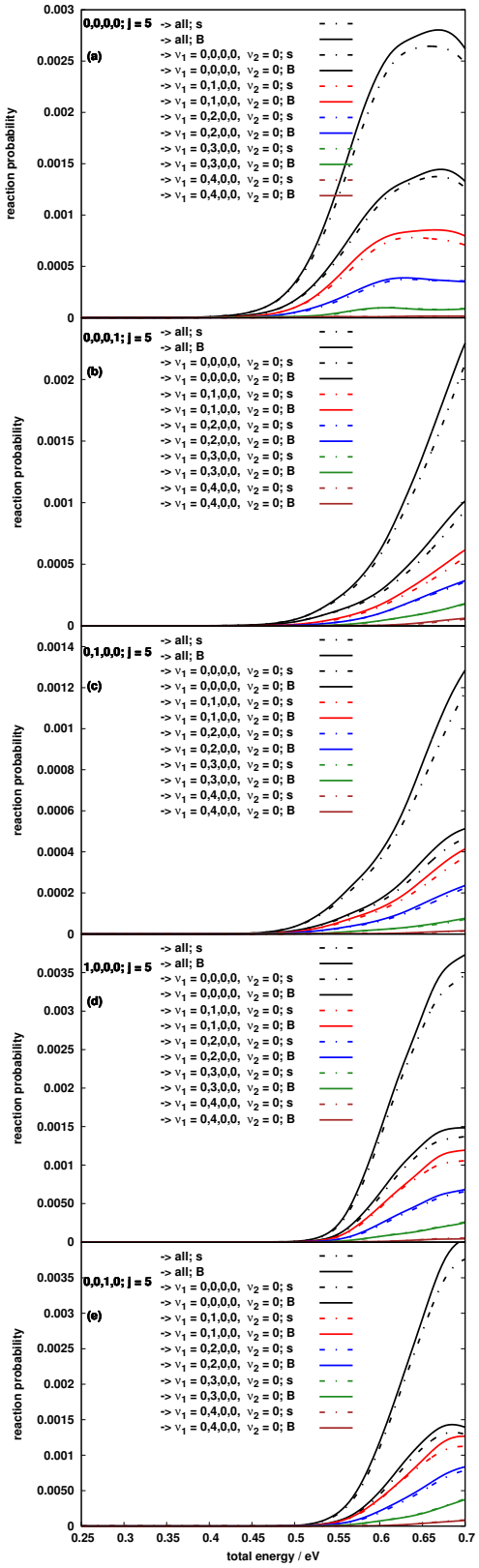

FIG. 9: State-to-state reaction probabilities $p_{\nu_{CH_3},\nu_{H_2}\leftarrow\nu_{CH_4},j=5}(E)$ and initial state-selected reaction probabilities $p_{\nu_{CH_4},j=5}(E)$ computed employing the SPF basis **C** (solid lines) and **s** (dashed lines)

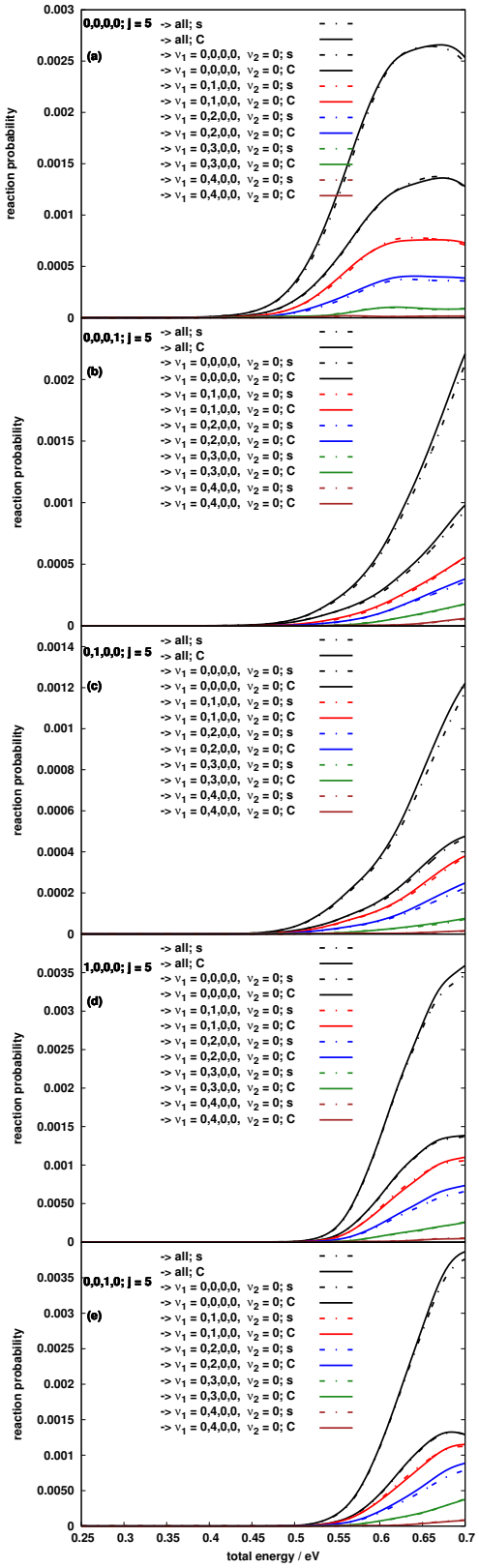

FIG. 10: State-to-state reaction probabilities $p_{\nu_{CH_3},\nu_{H_2}\leftarrow\nu_{CH_4},j=5}(E)$ and initial state-selected reaction probabilities $p_{\nu_{CH_4},j=5}(E)$ computed employing the SPF basis **D** (solid lines) and **s** (dashed lines)

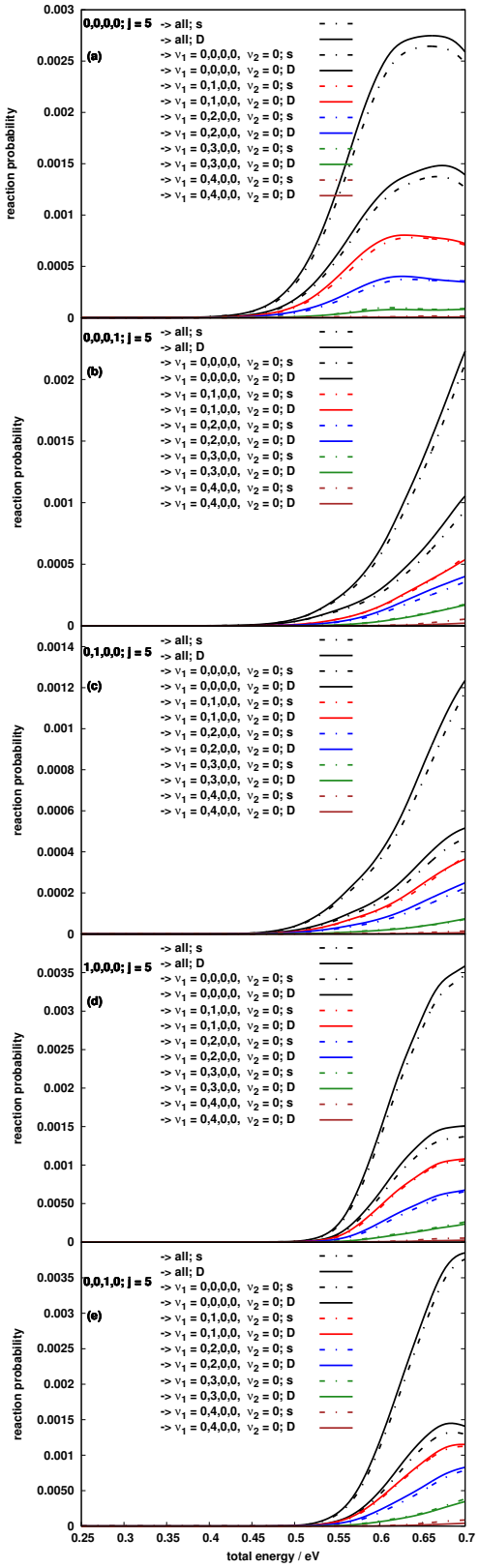

FIG. 11: State-to-state reaction probabilities $p_{\nu_{CH_3},\nu_{H_2}\leftarrow\nu_{CH_4},j=5}(E)$ and initial state-selected reaction probabilities $p_{\nu_{CH_4},j=5}(E)$ computed employing the SPF basis **E** (solid lines) and **s** (dashed lines)

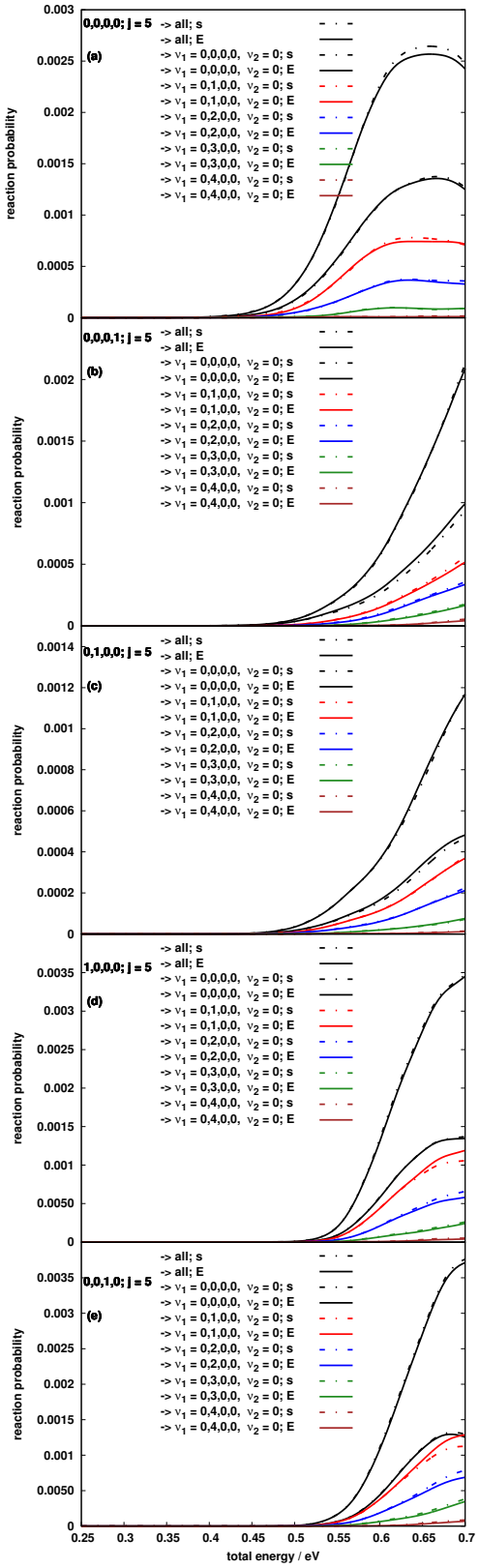

* Electronic address: rwelsch@uni-bielefeld.de

† Electronic address: uwe.manthe@uni-bielefeld.de

[1] Welsch, R.; Manthe, U.; Fast Shepard interpolation on graphics processing units: potential energy surfaces and dynamics for H+CH_4 →H_2 +CH_3, *J. Chem. Phys.,* **2013,** 138, 164118

[2] Welsch, R.; Manthe, U.; Communication: Ro-vibrational control of chemical reactivity in H+CH_4→ H_2+CH_3: full-dimensional q uantum dynamics calculations and a sudden model, *J. Chem. Phys.,* **2014,** 141, 051102

[3] Welsch, R.; Manthe, U.; The role of the transition state in polyatomic reactions: Initial state-s elected reaction probabilities of the H+CH_4→ H_2+CH_3 reaction, *J. Chem. Phys.,* **2014,** 141, 174313

[4] Schiffel, G.; Manthe, U.; Quantum dynamics of the H+CH_4 → H_2+CH_3 reaction in curvilinear coordinates: Full-dimensional and reduced dimensional calculations of reaction rates *J. Chem. Phys.,* **2010,** 132, 084103

[5] Evenhuis, C; Nyman, G.; Manthe, U.; Quantum dynamics of the CH_3 fragment: A curvilinear coordinate system and kinetic energy operators, *J. Chem. Phys.,* **2007,** 127, 144302

[6] Manthe, U.; A multilayer multiconfigurational time-dependent Hartree approach for quantum dynamics on general potential energy surfaces, *J. Chem. Phys.,* **2008,** 128, 164116

[7] Medvedev, D. M.; Harding, L. B.; Gray, S. K.; Methyl radical: ab initio global potential surface, vibrational levels and partition function, *Molecular Physics*, **2006,** 104, 73

[8] Boothroyd, A. I., Keogh, W. J.; Martin, P.G.; Peterson, M.R.; A refined H_3 potential energy surface, *J. Chem. Phys.*, **1996,** 104, 7139-7152